Pergamon

Cement and Concrete Research 30 (2000) 1023–1029

CEMENT AND CONCRETE RESEARCH

Quantitative Rietveld analysis of aluminous cement clinker phases

F. Guirado[a,*], S. Galí[b], S. Chinchón[c]

[a]*Servei de Recursos Científics, Univ. Rovira i Virgili, Plaça Imperial Tàrraco, 1, Tarragona, Catalonia 43005, Spain*
[b]*Dep. Cristallografia, Univ. Barcelona, Martí i Franquès s/n, Barcelona, Catalonia 08028, Spain*
[c]*Dep. Construccions Arquitectòniques, Univ. d'Alacant, Ap. Correus 99, Alacant 03080, Spain*

Received 15 December 1998; accepted 17 April 2000

Abstract

The mineralogical composition of high alumina cement (HAC) determines its ultimate properties once it has been mixed with water. The mineralogy of HAC cannot be given from the chemical composition because the thermodynamic equilibrium usually is not reached during the production process. The Rietveld method permits relatively quick quantitative phase analysis by fitting the calculated X-ray diffraction (XRD) profile with the observed one. Synthetic mixtures of pure phases were analyzed with this method in order to obtain a set of "empirical corrections" to be applied to samples of HAC clinker without previous chemical treatment. Chemical composition estimated from the weight percent of phases was in good agreement with composition obtained by X-ray fluorescence (XRF).

Keywords: X-ray diffraction; Calcium aluminate cement; Clinker; Amorphous material; Characterization

1. Introduction

Attempts of quantitative phase analysis of aluminous cements have been carried out by several methods: selective dissolution, electron microscopy, reflected light microscopy and powder X-ray diffraction (XRD) [1–3]. The latter method has been proved to be very promising.

Nowadays, most of quantitative phase analyses of aluminous cements using X-ray powder diffraction are based on the Chung [4–6] method and its modifications. This method is based on the integrated intensity ratios of selected peaks for each phase present and an internal standard in a mixture. It requires the preparation of mixtures of pure phases with the standard, in order to obtain the calibration constants. Intensity ratio methods are limited to the kind of mixtures previously prepared and do not take into account a variety of factors that affect the reproducibility of measured intensity as the preferred orientation of crystallites, the presence of solid solutions, peak overlapping and the presence of amorphous phases. Several authors have suggested to solve peak overlapping by deconvoluting the overlapped peaks as a sum of single peaks. This improvement solves only, in part, the problem because the percentage of each phase is based on the intensity ratios of a limited number of peaks. In fact, the methods using both, intensity ratios and partial profile fitting, appear to be an evolution of Chung's method towards Rietveld method.

2. Theoretical considerations

The Rietveld method was originally conceived for refining crystal structures using neutron [7] and, later, X-ray powder diffraction data [8]. The refinement consists of fitting the complete experimental diffraction pattern with a calculated profile and background and requires the knowledge of the crystal structure of all phases of interest. Eventually, one unknown structure can also be included in the refinement whenever their cell parameters are known. Common problems of quantitative phase analysis by XRD such as peak overlapping, preferred orientation and solid solutions are minimized with this method. The weight fraction (W_α) of each phase α is related with its scale factor (S_α) which is defined as [Eq. (1)]:

$$S_\alpha = \frac{W_\alpha \rho_m K}{V_\alpha^2 \rho_\alpha \mu_m}, \quad (1)$$

* Corresponding author. Tel.: +34-977-55-97-83; fax: +34-977-55-82-61.
E-mail address: fgg@src.urv.es (F. Guirado).

0008-8846/00/$ – see front matter
PII: S0008-8846(00)00289-1

Table 1
Real and estimated composition in pure phases of three synthetic mixtures: STD1, STD2 and STD3

		CA	$C_{12}A_7$	C_2AS	β-C_2S	C_4AF
STD1	real weight percent	52.0	7.0	8.0	4.0	29.0
	calculated weight percent	51.5(8)	5.9(4)	13.4(6)	4.2(3)	24.9(6)
R_p=10.9; R_{wp}13.8; χ^2=2.02	R_B	9.28	5.84	7.27	13.0	5.23
STD2	real weight percent	62.5	4.7	7.5	6.5	18.7
	calculated weight percent	61.4(6)	3.9(4)	12.2(6)	6.9(6)	15.5(4)
R_p=10.4; R_{wp}13.3; χ^2=2.72	R_B	7.79	8.06	7.18	11.9	6.00
STD3	real weight percent	45.0	15.0	8.0	12.0	20.0
	calculated weight percent	45.9(6)	12.3(4)	12.8(6)	11.0(6)	17.9(6)
R_p=11.2; R_{wp}13.8; χ^2=2.73	R_B	9.09	7.39	7.39	15.5	5.99
	m_α	0.989(5)	0.823(8)	1.62(2)	0.96(4)	0.86(1)

Conventional Rietveld agreement indexes are indicated (R_p, R_{wp}, χ^2 and R_B). The empirical corrections, $W_{cal,\alpha}=m_\alpha W_{real,\alpha}$, calculated for each phase (see text) are listed at the end.

where ρ_m and μ_m are the density and the linear X-ray absorption coefficient of the mixture; K is a constant that includes all the geometrical and physical constant factors affecting intensity and V_α is the unit cell volume of phase α. The scale factor is individually refined for each phase in the mixture. Finally, the weight fraction for each phase is obtained from [Eq. (2)]:

$$W_\alpha = \frac{S_\alpha (ZMV)_\alpha}{\sum_{\alpha=1}^{n} S_\alpha (ZMV)_\alpha} \quad (2)$$

where Z, M, V are the numbers of formula units per unit cell, mass of the formula unit and unit cell volume of

Table 2
Cell parameters (in Å) obtained from profile analysis for each phase present in commercial aluminous cement

		CES100	CES95	CES90	CES85
CA (Ref. [19])	*a*	8.708(1)	8.710(1)	8.711(1)	8.711(1)
	b	8.091(1)	8.0943(9)	8.0954(9)	8.0945(9)
	c	15.229(2)	15.233(2)	15.234(2)	15.232(2)
	β	90.18(1)	90.17(1)	90.18(1)	90.2(2)
	R_B	12.5	12.0	13.4	14.3
$C_{12}A_7$ (Ref. [20])	*a*	11.995(3)	11.997(3)	12.003(3)	12.000(3)
	R_B	14.5	12.7	12.1	13.6
C_2AS (Ref. [21])	*a*, *b*	7.726(8)	7.715(9)	7.726(9)	7.720(9)
	c	5.07(1)	5.09(1)	5.07(1)	5.07(1)
	R_B	11.3	7.7	9.5	9.7
β-C_2S (Ref. [22])	*a*	5.512(5)	5.511(6)	5.518(6)	5.518(7)
	b	6.755(9)	6.749(9)	6.747(9)	6.76(1)
	c	9.32(1)	9.32(1)	9.32(1)	9.31(1)
	β	94.47(9)	94.5(1)	94.5(1)	94.6(1)
	R_B	12.1	11.3	12.0	12.3
C_4AF (Ref. [23])	*a*	5.560(2)	5.560(2)	5.562(2)	5.560(2)
	b	14.655(4)	14.649(4)	14.653(4)	14.656(4)
	c	5.396(2)	5.398(2)	5.398(2)	5.398(1)
	R_B	10.9	13.3	10.4	10.4
Ca_2OAl_{32-2v} $Mg_vSi_vO_{68}$ (Ref. [16])	*a*	27.75(2)	27.80(2)	27.79(3)	27.79(3)
	b	10.804(7)	10.811(8)	10.812(9)	10.807(8)
	c	5.134(5)	5.131(6)	5.127(6)	5.128(6)
	R_B	13.4	10.6	12.0	12.5
CT (Ref. [24])	*a*	5.374(8)	5.374(8)	5.38(1)	5.37(1)
	b	5.387(8)	5.391(7)	5.37(2)	5.38(1)
	c	7.60(1)	7.593(8)	7.60(2)	7.60(2)
	R_B	8.5	7.1	7.5	8.8
Si	R_B	–	9.1	13.7	10.7
R_p		16.6	16.9	17.3	16.8
R_{wp}		20.9	21.4	21.7	20.6
χ^2		9.1	11.8	10.9	10.6

Whole conventional agreement indexes (R_p, R_{wp}, χ^2) and individual R_B are also given. (the esd is indicated between parentheses).

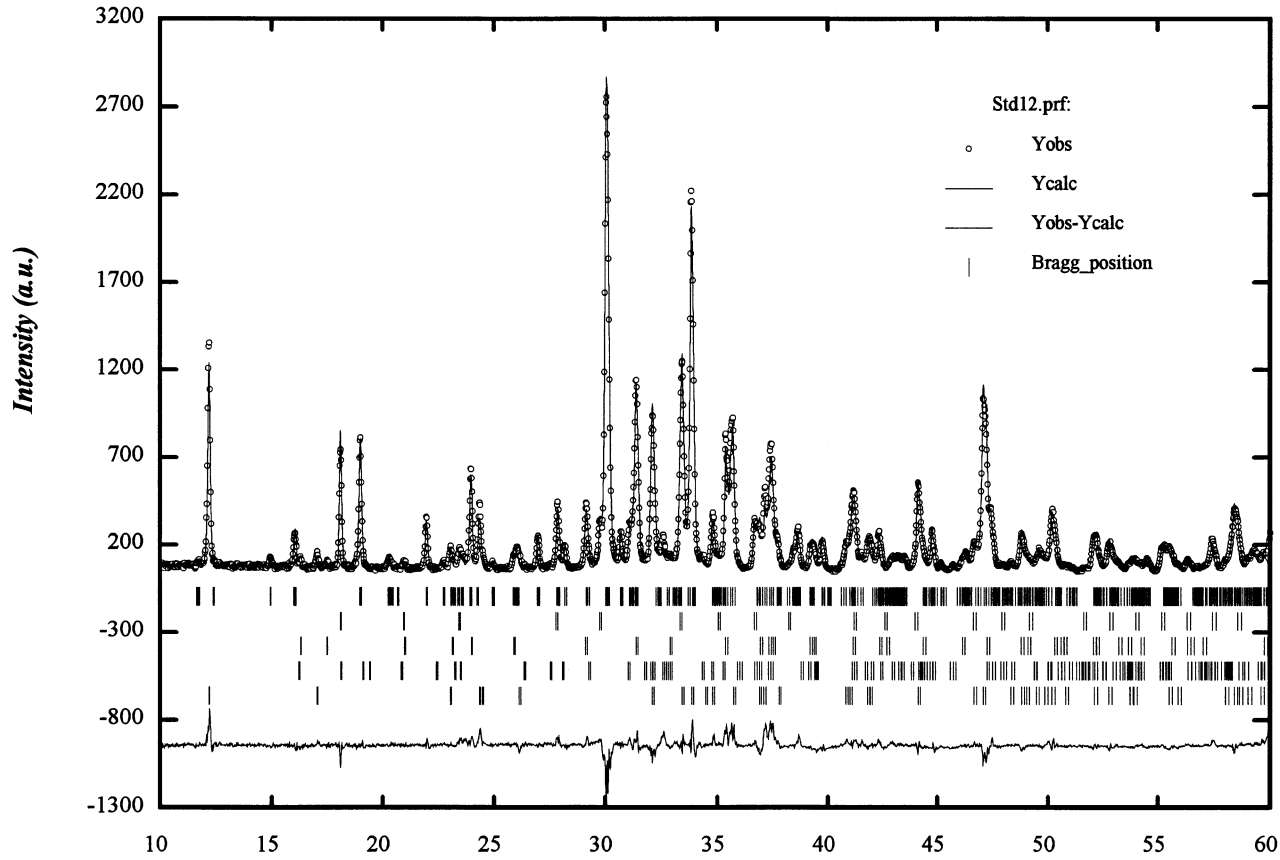

Fig. 1. Observed profile in circles, calculated profile in solid line, and the profile difference at the bottom for sample STD1. The position of Bragg reflections are also indicated for each phase present, from top to bottom: CA, $C_{12}A_7$, C_2AS, β-C_2S and C_4AF.

phase α in a mixture of n phases, respectively. Eq. (2) is valid assuming that all phases present in the sample are included in the analysis and there is not an amorphous portion present.

If one of the above conditions is not fulfilled, a known weight (W_s) of crystalline internal standard must be added to the sample. In this case, the relative weight fraction for each phase is calculated from [Eq. (3)]:

$$W_\alpha = \frac{W_s S_\alpha (ZMV)_\alpha}{S_s (ZMV)_s}. \quad (3)$$

Finally, the amorphous fraction (W_a) is calculated by difference from unity [Eq. (4)]:

$$W_a = 1 - W_s - \sum_{\alpha=1}^{n} W_\alpha. \quad (4)$$

The added internal standard plays the role of eliminating the uncertainty in the sum of crystalline weight fractions. Eventually, one minority undetected crystalline phase present in the mixture could be included in the amorphous weight fraction.

According to expression (3), the error in the estimated amount of phase α depends basically on the errors in the refined scale factors S_α and S_s. Other minor sources of error are the molecular weights and volume cells of phases when these are solid solutions.

Physical characteristics of the sample may give rise to microabsorption or extinction which influence the final value of S_α and S_s. In addition, the specimen preparation procedure may favour preferential orientation, especially when powder crystallites have anisotropic shape. Other sources of error in the estimated scale factor depend only on statistical considerations. Accepting that the diffraction profile has been measured with a wise combination in the selected step size with measuring time per step [9], the relative weight fractions W_α/W_s do not influence much the estimated errors in S_α and S_s. However, two extreme situations should be avoided. One is the dilution effect produced on the minority phases by a great amount of added standard. The other opposite situation is the addition of a poor amount of standard. In both cases, the low peak/background intensity ratio led to high errors in S_α and S_s, respectively.

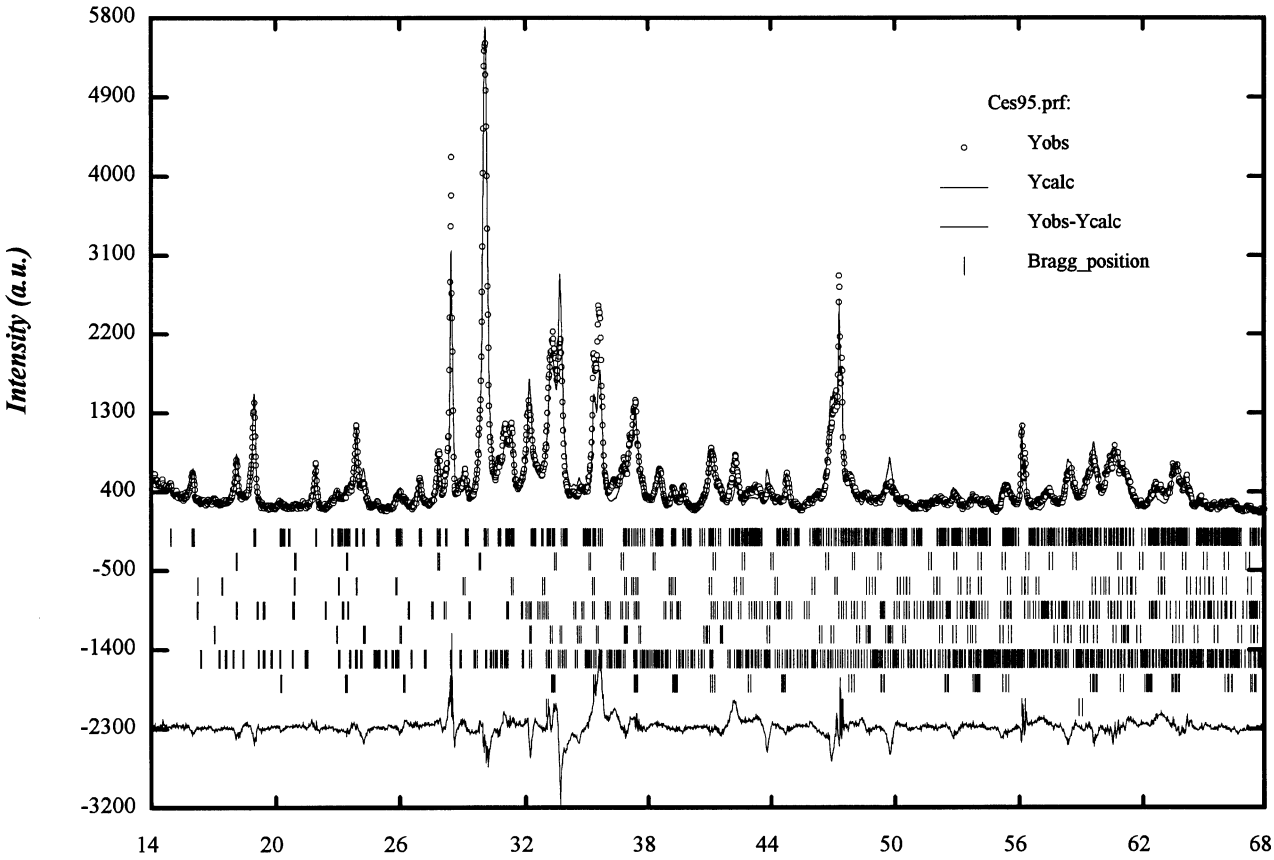

Fig. 2. Observed profile in circles, calculated profile in solid line, and the profile difference at the bottom for sample CES95. The position of Bragg reflections are also indicated for each phase present, from top to bottom: $CA_{1-x}F_x$, $C_{12}A_7$, C_2AS, β-C_2S, $C_2A_{1-x}F_x$, pleochroite, CT and Si.

It appears that there is an optimum W_s, which minimizes the errors in the estimated weights of all fractions. This value cannot be easily defined in advance, when the amount of each minority phase is still unknown. As a general rule, we recommend to repeat the measurement with different amount of standard.

With regards to the estimated error in the fraction of the amorphous phase, expression (4) indicates that $\sigma(W_a)$ would depend on the errors in W_α, W_β, etc., crystalline fractions. The general expression giving the standard deviation of a function in terms of those of the variables applied to Eq. (4) gives [Eq. (5)]:

$$\sigma(W_a) = \left(\sum_{\alpha=1}^{n} \sigma^2(W_\alpha) \right)^{1/2} . \quad (5)$$

The above expression tells us that the estimated error in the amorphous phase is bigger than those of crystalline phases.

3. Experimental

Pure phases CA, $C_{12}A_7$, C_2AS, β-C_2S and C_4AF were obtained from powder mixtures of $CaCO_3$, Al_2O_3, Fe_2O_3 and SiO_2 (PROLABO purity), with the suitable proportions. Each phase was sintered at the Lafarge Laboratories in a furnace using Pt crucibles and the optimum temperature was chosen according to usual procedures. The progress in the reaction was checked periodically by XRD until the reaction was complete. Pure phases were milled in a ring mortar and sieved below 40 μm. Three mixtures (STD1, STD2 and STD3) consisting of five pure phases were prepared by mixing CA, $C_{12}A_7$, C_2AS, β-C_2S and C_4AF in different proportions. The proportions were similar to those commonly expected in high alumina cement (HAC). Synthetic mixtures were homogenized in a ring mortar of tungsten carbide with cyclohexane (C_6H_{12}, PROLABO purity) in order to avoid the reaction of phases with water. Finally, all mixtures dried at 100°C were ready for XRD analysis. The composition of synthetic mixtures is listed in Table 1.

The HAC commercial clinker usually contains a glassy portion due to the production process, giving rise to a characteristic diffuse background in the XRD profile. In order to quantify the amorphous portion, we prepared another group of four samples with commercial Spanish HAC (fondu type and low alumina–high iron grade according to Scrivener and Capmas [10] classification). These samples were mixed with 0 wt.%, 5 wt.%, 10 wt.%

Table 3
Weight percent of phases present in commercial HAC calculated from Rietveld analysis.

Sample	Calculated	CA	$C_{12}A_7$	C_2AS	β-C_2S	C_4AF	Pleochroite	CT	Amorphous
CES100	(i)	52.4(7)	5.1(4)	3.6(4)	4.5(4)	21.5(9)	10.6(7)	2.3(2)	–
CES95	(ii)	51.6(2.5)	5.4(5)	2.9(4)	4.5(4)	20.7(1.4)	9.0(8)	3.1(2)	2.8(2.4)
CES90	(ii)	49.9(1.8)	5.1(4)	3.6(4)	4.7(4)	19.9(1.2)	9.1(8)	2.3(2)	5.4(1.9)
CES85	(ii)	50.1(1.7)	5.0(4)	3.5(4)	3.9(4)	20.4(1.2)	9.2(8)	2.1(2)	5.9(1.9)
CES100	(iii)	50.9(8)	5.9(5)	2.1(2)	4.5(5)	24.2(6)	10.2(7)	2.2(2)	–
CES95	(iii)	51.5(2.9)	6.4(6)	1.8(2)	4.6(5)	23.8(1.8)	8.9(9)	3.0(2)	–
CES90	(iii)	51.4(2.4)	6.1(6)	2.2(3)	5.1(5)	23.5(1.6)	9.3(8)	2.4(2)	–
CES85	(iii)	51.6(2.3)	6.2(6)	2.2(3)	4.1(5)	24.3(1.6)	9.4(8)	2.2(2)	–

The calculated weight percent values are indicated for each sample according to four different calculation (the esd is indicated between parentheses)
(i) Weight percent of phases calculated from Eq. (2).
(ii) Weight percent corrected calculating the amorphous part with the internal standard (Eq. (4).
(iii) Weight percent corrected by applying the empirical corrections calculated to STD1, STD2 and STD3.

and 15 wt.% of Si (NBS 640b) used as standard (samples labelled CES100, CES95, CES90 and CES85, respectively). The homogenizing procedure was the same as for synthetic mixtures.

The XRD intensities of all samples were measured at room temperature in a Siemens-D500 powder diffractometer using CuKα radiation and a secondary graphite monochromator. Samples were placed in a backmounted sampler holder to avoid the preferred orientation of the crystallites [11]. Special analytical conditions (step size 0.02°, time per step 16 s) were used in order to obtain experimental diffraction profiles with low statistical errors, suitable for Rietveld analysis. Small aperture slits were used to avoid the contribution of the sample holder to the X-ray diffractogram.

4. Results and discussion

Pattern fitting was done by means of the program, FULLPROF [12], which is based on the Rietveld method. Rietveld refinement was applied over the entire measured profile (10–60° 2θ). The background for each diffraction pattern was defined as the interpolation of n points introduced manually. The profile function used was Pearson VII and the peak asymmetry correction proposed by Bérar and Baldinozzi [13] was used. Zero shift, individual scale factor and cell parameters were the only refined parameters during the first stage of the refinement, until an apparent convergence was reached. After this, the phase profile parameters (U, V and W), M coefficient, and two asymmetry parameters were included until final convergence. A maximum of 32 parameters were refined.

Accurate phase identification of commercial HAC (sample CES100) gave the following phases and solid solutions: $CA_{1-x}F_x$, $C_{12}A_7$, C_2AS, β-C_2S, $C_2A_{1-x}F_x$, $Ca_{20}Al_{32-2v}Mg_vSi_vO_{68}$ (pleochroite or Q-phase) and CT (perovskite). References giving cell parameters and atomic coordinates of all phases involved in the refinements are given in Table 2.

The method was tried initially with three synthetic mixtures with five pure and crystalline phases. (STD1, STD2 and STD3). The calculated weight percent (Eq. (2)) for each phase in these samples is shown in Table 1 together with the conventional Rietveld agreement indexes (R_{wp}, R_w, χ^2 and R_B) of the profile fitting. The observed and calculated profile for sample STD1 is plotted in Fig. 1.

It is well known that the different X-ray absorption and anisotropic shapes of particles together with other minor effects produce systematic deviations of calculated values that frequently cannot be compensated. For this reason, we have introduced an empirical correction for each phase,

Table 4
Weight percent of simple oxides for studied samples of commercial HAC calculated from weight percent of phases according to two different calculations: (ii) and (iii). The weight percent of oxides obtained by XRF of the sample CES100 are listed at the bottom

	CaO	Al_2O_3	Fe_2O_3	SiO_2	MgO	TiO_2	P_2O_5	K_2O	MnO
CES100-i	39.0	43.6	12.4	3.1	0.5	1.4	–	–	–
CES95-ii	38.9	43.5	12.3	2.9	0.4	1.8	–	–	–
CES90-ii	39.0	43.0	12.1	3.3	0.4	1.4	–	–	–
CES85-ii	38.9	43.6	12.5	3.0	0.5	1.3	–	–	–
CES100-iii	39.0	42.4	13.5	2.9	0.5	1.3	–	–	–
CES95-iii	39.4	41.9	13.4	2.7	0.4	1.8	–	–	–
CES90-iii	39.3	42.5	13.2	3.0	0.4	1.4	–	–	–
CES85-iii	39.2	42.6	13.5	2.6	0.4	1.3	–	–	–
XRF	38.3(1)	39.3(2)	14.3(1)	2.6(1)	0.40(1)	1.56(1)	0.05(1)	<0.01	<0.01

m_α, obtained by linear regression from the relation $W_{cal,\alpha} = m_\alpha W_{real,\alpha}$ in each standard sample. The m_α values obtained are given in Table 1.

It can be seen that, apart from CA phase, the estimated values of all the remainder minority phases systematically deviate from the true values. Phases with $m_\alpha > 1$ have a tendency to be overestimated and phases with $m_\alpha < 1$ have a tendency to be underestimated. According to the theory, when the linear absorption coefficient of a phase in a mixture increases, the weight fraction obtained for this phase is more underestimated. However, we have not observed any simple relation between empirical factors and linear absorption coefficient, μ_α (using CuKα radiation and considering a powder density $\rho_{powder} = 0.8\rho_{crystal}$, we obtain for CA: 147.6; $C_{12}A_7$: 158.2; C_2AS: 164.5; β-C_2S: 237.7 and C_4AF: 392.7 cm^{-1}). The complex dependence of the empirical factor m_α, μ_α and $W_{real,\alpha}$ deserves a more detailed investigation.

The second step was to apply the method to commercial HAC samples. All phases present in HAC display some degree of solid solution that slightly modifies their XRD profiles, in special peak positions and relative intensities. These changes must be assumed and corrected in Rietveld analysis when the variation of cell parameters through solid solution is known. The iron content of $CA_{1-x}F_x$ and $C_2A_{1-x}F_x$ was calculated from the variation parameters proposed by Guirado et al. [14,15], and the brownmillerite structure type was assumed for $C_2A_{1-x}F_x$. The following composition was then estimated for these two solid solutions: $CaAl_{1.90}Fe_{0.09}O_4$ and $Ca_2Al_{0.51}Fe_{1.49}O_5$. The corresponding calculated molecular weights for these two solid solutions were introduced in Eq. (2). It is well reported that $C_2A_xF_{1-x}$ can also incorporate Mg, Si, Ti, Mn and Cr in its structure, but in our case, we did not consider this possibility in order to simplify the problem. The other phases present were considered to be pure and the composition of pleochroite phase was that proposed by Hanic et al. [16] as $Ca_{20}Al_{32-2\nu}Mg_\nu Si_\nu O_{68}$ with $\nu = 3$. The presence of the perovskite phase in HAC had been already reported [17] and it has been recently shown by HRTEM images that there is a nanometric intergrowth between perovskite and brownmillerite structures [18]. The observed and calculated profile for sample CES95 having 5 wt.% of Si as internal standard is plotted in Fig. 2.

The refinement of minor phases with very similar cell parameters and structures (see, for instance, brownmillerite and perovskite; Table 2) is very difficult, leading to a high correlation between scale factors, which give different quantitative results for these phases even if the agreement indices of the refinement are the same. Since most titanium and iron are concentrated in the perovskite and brownmillerite, respectively, the correlation between scale factors is translated to the calculated amounts of titanium and iron oxides.

Table 2 shows the calculated cell parameters for each phase present in commercial samples. Rietveld conventional agreement indexes are also indicated. The calculated weight percent values of phases are listed in Table 3 according to three different cases:

(i) weight percent calculated directly from Eq. (2);
(ii) weight percent corrected by calculating the amorphous part with the internal standard (Eq. (4));
(iii) weight percent calculated directly from Eq. (2) and corrected by applying the empirical corrections to STD1, STD2 and STD3. The correction was applied for all phases present except pleochroite.

According to the theory, the addition of Si standard (μ_{Si}: 113 cm^{-1}) does not affect the estimated weight percent of phases, indicating that the dilution of the sample in small amounts of the added standard does not perturb considerably the results (see CES95-ii, CES90-ii and CES85-ii). In any case, the differences are around ±0.5%. The amorphous part of this cement was estimated to be 5.6% (±2).

The weight percent of each phase is slightly modified (see CES100-iii, CES95-iii, CES90-iii and CES85-iii) by applying the empirical corrections previously determined to synthetic mixtures (STD1, STD2 and STD3). According to this, the weight percent values of CA and C_2AS are lower; $C_{12}A_7$ and C_4AF weight percent increases and β-C_2SCT and pleochroite phases remain unmodified.

The content in simple oxides of the same commercial HAC was analyzed in order to check the validity of the method employed. The resulting pearls were analyzed by X-ray fluorescence (XRF) in a sequential spectrometer Philips PW 1400 with Rh radiation. The composition is shown in Table 4. The same table shows the weight percent of simple oxides calculated from the weight percent of each phase in Table 3. The results show a good agreement between the composition indirectly calculated from Rietveld analysis and that obtained by XRF. The Al_2O_3 weight percent is lower by XRF than by XRD but the CaO content is the same. The Fe_2O_3 weight percent is the same in both methods if we consider the sum of Fe_2O_3+TiO_2. The composition of the undetected portion is unknown, and therefore, was not included in the calculation.

The differences between the estimated composition before and after the application of the empirical corrections are small but cannot be neglected, especially for Fe_2O_3 and SiO_2.

5. Conclusions

The weight percent values of phases calculated from Rietveld analyses are always subjected to small systematic errors due to ubiquitous solid solution in these phases. For the well-characterized solid solutions, the composition of the phases can be estimated from the refined cell parameters,

and included in the calculations, improving the results. Other sources of error like microabsoption, anisotropic shape of crystallites, high correlation between structural parameters, etc., could not be completely compensated in the used model of profile fitting. The weight percent of phases calculated may then be slightly corrected using empirical corrections. These empirical corrections can only be applied when all the experimental conditions are held constant.

The addition of an internal standard allows the estimation of the vitreous portion and possibly crystalline phases not detected by XRD. In the present case, optimum amounts of internal standard appear to be around 10–15 wt.%.

The concentration of titanium and iron in minority phases with similar cell parameters creates unfavourable conditions for estimating the amount of these oxides in the sample. Apart from this difficulty, the composition in oxides calculated from quantitative of phases agrees fairly well with those obtained by XRF. The best agreement is obtained by CaO content, because calcium atomic positions are not substituted significantly by other cations.

The iron content of $CA_{1-x}F_x$ s.s. and $C_2A_{1-x}F_x$ s.s. has been estimated from previous works and the modified molecular weight introduced in the phase content calculation. In this sense, it is convenient to characterize accurately all phases present before applying the Rietveld method.

The employed method reveals a good precision, taking into account the reproducibility of results from samples with different dilutions, and good accuracy by comparing the composition with XRF.

Acknowledgments

The authors thank Dr. F. Sorrentino from Lafarge Laboratories for providing pure cement phases and Dr. K. Scrivener for useful comments. We also thank Serveis Cientifico Tècnics of the Universitat de Barcelona for the XRD and XRF analyses. This study received financial support from the Spanish Government, project MAT97-0380.

References

[1] L.J. Struble, Quantitative phase analysis of clinker using X-ray diffraction, Cem Concr Aggregates 13 (2) (1991) 97–102.
[2] L. Redler, Quantitative X-ray diffraction analysis of high alumina cements, Cem Concr Res 21 (1991) 873–884.
[3] H.G. Midgley, Quantitative determination of phases in high alumina cement clinkers by X-ray diffraction, Cem Concr Res 6 (1976) 217–224.
[4] F.H. Chung, Quantitative interpretation of X-ray diffraction patterns of mixtures: I. Matrix flushing method for quantitative multicomponent analysis, J Appl Crystallogr 7 (1974) 526.
[5] F.H. Chung, Quantitative interpretation of X-ray diffraction patterns of mixtures: II. Adiabatic principle of X-ray diffraction analysis of mixtures, J Appl Crystallogr 7 (1974) 519–525.
[6] F.H. Chung, Quantitative interpretation of X-ray diffraction patterns of mixtures: III. Simultaneous determination of a set of reference intensities, J Appl Crystallogr 8 (1975) 17–19.
[7] H.M. Rietveld, A profile refinement method for nuclear and magnetic structures, J Appl Crystallogr 2 (1969) 65–71.
[8] D.B. Wiles, R.A. Young, A new computer program for Rietveld analysis of X-ray powder diffraction patterns, J Appl Crystallogr 14 (1981) 149–151.
[9] R.J. Hill, I.C. Madsen, The effect of profile step width on the determination of crystal structure parameters and estimated standard deviations by X-ray Rietveld analysis, J Appl Crystallogr 19 (1986) 10–18.
[10] K.L. Scrivener, A. Capmas, Calcium aluminate cements, LEA's Chemistry of Cement, 4th edn. Arnold Publishers, London, 1998, p. 713.
[11] D.L. Bish, R.C. Reynolds, Sample preparation for X-ray diffraction, in: D.L. Bish, J.E. Post (Eds.), Modern Powder Diffraction, The Mineralogical Society of America, Washington, DC, 1989, pp. 73–97.
[12] J. Rodríguez-Carvajal, Abstracts of the Satellite Meeting on Powder Diffraction on the 15th Congress of the IUCr, Toulouse, IUCr (1990) 127.
[13] J.-F. Bérar, G. Baldinozzi, Modeling of line-shape asymmetry in powder diffraction, J Appl Crystallogr 26 (1993) 128–129.
[14] F. Guirado, S. Galí, J.S. Chinchón, The crystallography of $CA_{1-x}F_x$ using X-ray powder diffraction techniques, Cem Concr Res 24 (5) (1994) 923–930.
[15] F. Guirado, S. Galí, J.S. Chinchón, X-ray profile analysis of $Ca_2Fe_{2-x}Al_xO_5$ solid solutions, World Cem 27 (12) (1996) 73–76.
[16] F. Hanic, M. Handlovic, I. Kapralik, The structure of a quaternary phase $Ca_2OAl_{32-2v}Mg_vSi_vO_{68}$, Acta Crystallogr 36B (1980) 2863–2869.
[17] H. Motzet, H. Poellmann, Quantitative phase analysis of high alumina cements, Proc Int Congr Cem Microsc, Guadalajara, México, 1998 187–206.
[18] K.L. Scrivener, personal communication, 1998.
[19] W. Hörkner, H.K. Müller-Buschbaum, Zur kristallstruktur von $CaAl_2O_4$, J Inorg Nucl Chem 38 (1976) 983–984.
[20] A.N. Christensen, Neutron powder diffraction profile refinement studies on $Ca_{11.3}Al_{14}O_{32.3}$ and $CaClO(D_{0.88}H_{0.12})$, Acta Chem Scand 41 (1987) 110–112.
[21] M. Kimata, N. Ii, The structural property of synthetic gehlenite, Neues Jahrb Mineral, Monatsh 143 (1982) 254–267.
[22] K.H. Jost, B. Ziemer, R. Seydel, Redetermination of beta-dicalcium silicate, Acta Crystallogr 33B (1977) 1696–1700.
[23] A.A. Colville, S. Geller, The crystal structure of brownmillerite, Ca_2FeAlO_5, Acta Crystallogr 27B (1971) 2311–2315.
[24] S. Sasaki, C.T. Prewitt, J.D. Bass, Orthorombic perovskite $CaTiO_3$ and $CdTiO_3$: Structure and space group, Acta Crystallogr 43C (1987) 1668–1674.